## SCIENCE CHINA Chemistry



## COMMUNICATIONS

June 2021 Vol.64 No.6: 948–952 https://doi.org/10.1007/s11426-020-9952-x

## Solvent-driven reversible transformation between electrically neutral thiolate protected Ag<sub>25</sub> and Ag<sub>26</sub> clusters

Yu-Ling Tan<sup>1,2</sup>, Ling Yang<sup>1</sup>, Tian-Chen Yu<sup>3</sup>, Hong Yu<sup>1\*</sup>, Xin-Yao Wang<sup>1</sup>, Ying-Lin Song<sup>3</sup>, Zheng Niu<sup>1\*</sup> & Jian-Ping Lang<sup>1,2\*</sup>

<sup>1</sup>College of Chemistry, Chemical Engineering and Materials Science, Soochow University, Suzhou 215123, China;
<sup>2</sup>State Key Laboratory of Organometallic Chemistry, Shanghai Institute of Organic Chemistry, Chinese Academy of Sciences,
Shanghai 200032, China;

<sup>3</sup>School of Physical Science and Technology, Soochow University, Suzhou 215006, China

Received December 27, 2020; accepted January 29, 2021; published online April 2, 2021

Two atom-precise silver nanoclusters  $[Ag_{25}Cl_2(Tab)_{14}(PhCOO)_{11}(DMF)_4](PF_6)_{12}$   $(Ag_{25}, DMF=N,N-dimethylformamide)$  and  $[Ag_{26}Cl_2(Tab)_{14}(PhCOO)_{13}(DMAc)_4](PF_6)_{11}$   $(Ag_{26}, DMAc=N,N-dimethylacetamide)$  were synthesized based on the electrically neutral thiolate protective ligand, 4-(trimethylammonio)benzenethiolate (Tab). The weak Ag-S interaction in Tab-protected silver nanoclusters allows to insert or leave a single silver atom in the Ag-S skeleton through solvent-trigger core fragmentation and re-arrangement, thereby realizing the reversible conversion of  $Ag_{25}$  and  $Ag_{26}$  for the first time.

silver nanocluster, electrically neutral thiolate, reversible transformation

Citation: Tan YL, Yang L, Yu TC, Yu H, Wang XY, Song YL, Niu Z, Lang JP. Solvent-driven reversible transformation between electrically neutral thiolate protected Ag<sub>25</sub> and Ag<sub>26</sub> clusters. Sci China Chem, 2021, 64: 948–952, https://doi.org/10.1007/s11426-020-9952-x

Ligand-stabilized silver nanoclusters have attracted wide attention in the past few decades owing to their aesthetic structures and potential applications in luminescence, catalysis, and biosensing fields [1]. In recent years, the flourishing development of the anion-template method and the geometric polyhedral principle has pushed the self-assembly of silver nanoclusters to a remarkable level [2]. A series of the ligand-protected (*e.g.*, thiolate, phosphine, and alkynyl) silver nanoclusters with atomic precision have been isolated [3], which provide an opportunity to observe and study the configuration transformation of the silver nanoclusters at the atomic level [4].

Since the complex structure of metal nanoclusters and the difficulty in structure control, the transformation of metal nanoclusters under external stimuli still faces great challenge. The flexible coordination mode of silver atoms makes the reversible structural changes of silver nanoclusters be difficult [5]. The previous studies have proved that the silver nanoclusters with the same number of silver atoms can achieve reversible structural transformation by outside stimuli [6,7]. For example, Zang and co-workers [7] indicated that the Ag<sub>12</sub>@POSS<sub>6</sub> cluster undergoes a two-way core transformation from cubic octahedron to normal cubic octahedron driven by different solvents. Recently, Wang et al. [8] reported that silver nanoclusters  $[Ag_{21}(dpa)_{12}]SbF_6$  and [Ag<sub>22</sub>(dpa)<sub>12</sub>](SbF<sub>6</sub>)<sub>2</sub>, (dpa=dipyridylamido) with a different number of silver atoms can also be inter-converted via adding or removing a silver atom on the surface of the core structure Ag<sub>13</sub> under the triggered-solvents. However, the composition and configuration of core Ag<sub>13</sub> constantly remain invariable upon structural transformation. To date, few studies can realize the reversible core structural transformation with the changes of the number of silver atoms, be-

<sup>\*</sup>Corresponding authors (email: yuhong@suda.edu.cn; nkniuzheng@163.com; iplang@suda.edu.cn)

cause the core skeleton of most of the reported ligand-protected metal nanoclusters are generally quite stable [9]. Therefore, achieving the structure transformation between two similar Ag clusters is a big challenge.

Different from the thiolate ligands with negative monovalent commonly used in the general synthesis of silver nanoclusters, Tab (4-(trimethylammonio) benzenethiolate) [10] is a unique electrically neutral thiolate. Our previous work indicated that the special electrical properties of Tab can lead to the relatively weak interaction between Ag<sup>+</sup> and S<sup>2-</sup> compared with the Ag-S interactions in most of the other thiolate-protected silver nanoclusters [4e,11]. Therefore, the skeleton of Tab protected silver nanoclusters would be changed through external stimulation (Figure 1). In this regard, we employed the Tab-protected silver nanoclusters as a model to investigate the solvent-driven core structure transformation with the changes in the number of silver atoms.

Herein, we used Tab as the protected ligand and combined solvents of similar functionalities to construct two novel nanoclusters with a similar Ag-S skeleton: [Ag<sub>25</sub>Cl<sub>2</sub>(Tab)<sub>14</sub>- $(PhCOO)_{11}(DMF)_4](PF_6)_{12}$   $(Ag_{25}, DMF=N,N-dimethylfor$ mamide) and  $[Ag_{26}Cl_2(Tab)_{14}(PhCOO)_{13}(DMAc)_4](PF_6)_{11}$ ( $Ag_{26}$ , DMAc=N,N-dimethylacetamide). Interestingly, a single silver ion can be inserted into the core skeleton of  $Ag_{25}$ under the DMAc and CH<sub>3</sub>CH<sub>2</sub>OH trigger, resulting in a crystalline cluster Ag<sub>26</sub>. Furthermore, a silver atom at the same site can be removed from the core skeleton of  $Ag_{26}$  to regenerate complex Ag<sub>25</sub> via the stimulation of mixed solvents DMF and CH<sub>2</sub>Cl<sub>2</sub>. The interesting reversible interconversion between  $Ag_{25}$  and  $Ag_{26}$  was realized through simple solvent molecular exchange and solvent-triggered core fragmentation and re-arrangement, which was confirmed by single-crystal X-ray diffraction (SCXRD), powder X-ray diffraction (PXRD), and electrospray ionization mass spectrometry (ESI-MS) measurements.

Ag<sub>25</sub> was prepared by the reaction of TabHPF<sub>6</sub>, PhCOOAg and KCl in a mixed solvent of DMF and CH<sub>2</sub>Cl<sub>2</sub> in a Teflon autoclave at 60 °C for 20 h. The yellow block crystals of Ag<sub>25</sub> were obtained through the diffusion method (Supporting Information online). SCXRD analysis revealed that Ag<sub>25</sub> crystallized in the triclinic space group  $P\overline{1}$  and the asymmetric unit contains a whole cluster.  $Ag_{25}$  cluster consists of 25 Ag atoms, 14 Tab ligands, 2 Cl<sup>-</sup>, 11 PhCOO<sup>-</sup> ligands, and 4 coordinated DMF molecules, with the Ag...Ag contacts lying in 2.850–3.428 Å (Figure 2(a), and Figures S1 and S2, Supporting Information online). The Ag-S skeleton of the core structure in the  $Ag_{25}$  cluster can be considered as a tumbler composed of cage A1 and cage B1 through sharing 4 silver atoms. As presented in Figure 2(c), cage A1 is composed of 17 Ag atoms and 8 S atoms on Tab ligands. The eight Tab ligands in cage A1 adopt a μ<sub>4</sub>-η<sup>1</sup>:η<sup>1</sup>:η<sup>1</sup>:η<sup>1</sup> mode stabilized Ag<sub>17</sub> skeleton, with the Ag-S bond lengths being

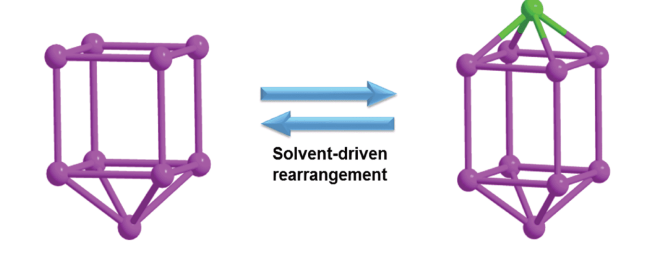


**Figure 1** Solvent-driven reversible transformation of Tab-protected silver nanoclusters with a different number of silver atoms. Pink and bright green spheres represent silver atoms (color online).

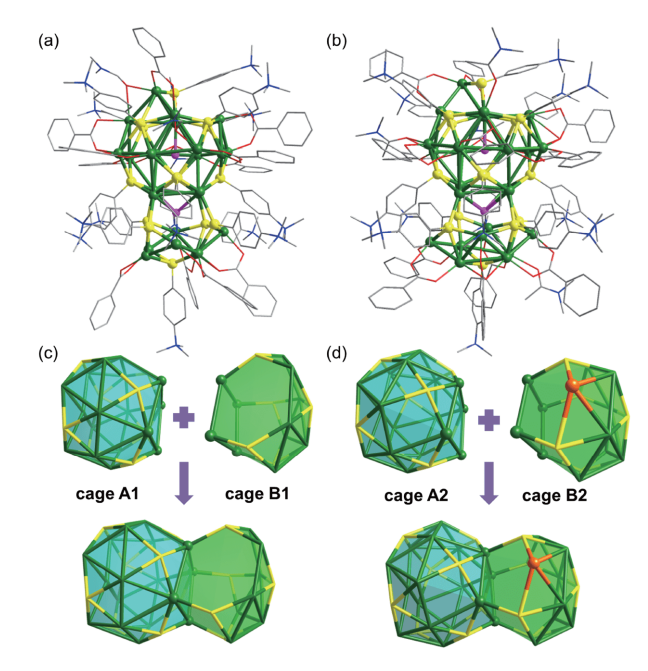


**Figure 2** Molecular structure of  $Ag_{25}$  (a) and  $Ag_{26}$  (b). Structural dissection of core Ag–S skeleton of  $Ag_{25}$  (c) and  $Ag_{26}$  (d), other parts are all omitted for clarity. Color codes: green, orange, Ag; yellow, S; blue, N; red, O; Pink, Cl; gray, C (color online).

in the range of 2.444 to 2.762 Å. Cage B1 is made up of 7 Ag atoms and 5 S atoms on Tab ligands. Three-fifths of the Tab ligands in cage B1 adopt a  $\mu_3$ - $\eta^1$ : $\eta^1$ : $\eta^1$ : $\eta^1$  coordination mode, while others take a  $\mu_4$ - $\eta^1$ : $\eta^1$ : $\eta^1$ : $\eta^1$  coordination mode, with the Ag–S bond lengths of 2.408–2.610 Å. One of the Ag<sub>3</sub> face on the core structure of  $Ag_{25}$  is covered by a silver atom, which is located at the bottom left of the top of cage A1 (Figure S3).

The surface of cage A1 is stabilized by 7 PhCOO ligands, a Tab ligand, and 4 DMF molecules, while cage B1 is protected by 4 PhCOO ligands (Figures S1 and S2). Furthermore, there exist two Cl ions, which act as the terminal and bridging ligands to stabilize the cage A1 and B1 through a  $\mu$ - $\eta^1$  mode and a  $\mu_4$ - $\eta^1$ : $\eta^1$ : $\eta^1$  mode, respectively (Figure S4).

Unique electrically neutral of the Tab molecule makes the Ag–Ag bonds in  $Ag_{25}$  is not very stable. Therefore, the change of the coordinated solvent molecules would lead to

the fracture and regeneration of the Ag-Ag bond. In this regard, we employed different solvent molecules to substitute the coordinated DMF molecules on Ag<sub>25</sub>, thus realizing the formation of the new Ag clusters. Through using the mixed solvents of DMAc and CH<sub>3</sub>CH<sub>2</sub>OH to replace DMF and CH<sub>2</sub>Cl<sub>2</sub> solvents, we obtained a new cluster Ag<sub>26</sub> (Supporting Information online). The single-crystal structural analysis revealed that Ag<sub>26</sub> crystallized in the monoclinic space group  $P2_1/n$  and contains 26 Ag atoms, 14 Tab ligands, 2 Cl<sup>-</sup>, 13 PhCOO<sup>-</sup> ligands, and 4 DMAc molecules, with the Ag...Ag contacts being in the range of 2.821– 3.469 Å (Figure 2(b), Figures S1 and S2). Although the number of silver atoms in Ag<sub>26</sub> is different from Ag<sub>25</sub>, the Ag-S skeletons of  $Ag_{26}$  and  $Ag_{25}$  are similar. The Ag-S skeleton of the core structure in  $Ag_{26}$  can be regarded as the combination of the two cages (cage A2 and cage B2), through sharing 4 silver atoms (Figure 2(d)). The number of  $Ag^+$  ions and  $S^{2-}$  ions that made up cage A2 in  $Ag_{26}$  is the same as that of  $Ag_{25}$ , and the Tab ligands of the two cages adopt the  $\mu_4$ - $\eta^1$ : $\eta^1$ : $\eta^1$ : $\eta^1$  coordination mode. Besides, the average bond length of Ag-S of cage A2 is 2.542 Å, which is similar to the value of cage A1 in the  $Ag_{25}$  cluster (2.536 Å). The further analysis of the skeleton of  $Ag_{25}$  and  $Ag_{26}$  showed that cage A1 in  $Ag_{25}$  is the same as cage A2 in  $Ag_{26}$ , while the Ag-S skeleton of cage B2 in Ag<sub>26</sub> has an additional Ag atom compared with the cage B1 in  $Ag_{25}$ . Cage A2 is stabilized by 8 PhCOO ligands, a Tab ligand, and 3 DMAc molecules, while cage B2 in Ag<sub>26</sub> is coordinated by 5 PhCOO ligands, and 1 DMAc molecule (Figures S1 and S2). Similar to Ag<sub>25</sub>, the two Cl<sup>-</sup> anions in the  $Ag_{26}$  adopt  $\mu$ - $\eta^1$  and  $\mu_4$ - $\eta^1$ : $\eta^1$ : $\eta^1$ : $\eta^2$ coordination modes to stabilize the Ag-S skeleton.

Remarkably, although the reagent chemicals used in the self-assembly synthesis process of clusters  $\mathbf{Ag_{25}}$  and  $\mathbf{Ag_{26}}$  are achiral, the arrangement of Ag, S, and Cl atoms leads to the two inherent chiral silver clusters (Figure 3) [12]. In the crystals of the  $\mathbf{Ag_{25}}$  and  $\mathbf{Ag_{26}}$ , the paired enantiomers of the two clusters are crystallized in one unit cell with a 1:1 stoichiometry, thus giving the racemic crystals (Figure S5). Unfortunately, we have not achieved chiral split through many attempts.

The comprehensive analysis of the synthesis method and single crystal structure of the two clusters reveal that the different coordinated solvent molecules between  $\mathbf{Ag_{25}}$  and  $\mathbf{Ag_{26}}$  are the key difference between their structures. In this regard, we tried to utilize the solvent stimuli method to achieve structural transformation between  $\mathbf{Ag_{25}}$  and  $\mathbf{Ag_{26}}$ . Upon dissolving the crystals of  $\mathbf{Ag_{26}}$  in a mixed solvent of DMF and  $\mathbf{CH_2Cl_2}$ , the solution got gradually changed from yellow to brown (Figure S7). After that, the high-quality yellow block crystals can be obtained by diffusion with diethyl ether. The following single crystal structural analysis revealed that the yellow crystals were  $\mathbf{Ag_{25}}$ . To investigate the transformation from  $\mathbf{Ag_{25}}$  back to  $\mathbf{Ag_{26}}$ , we induced the

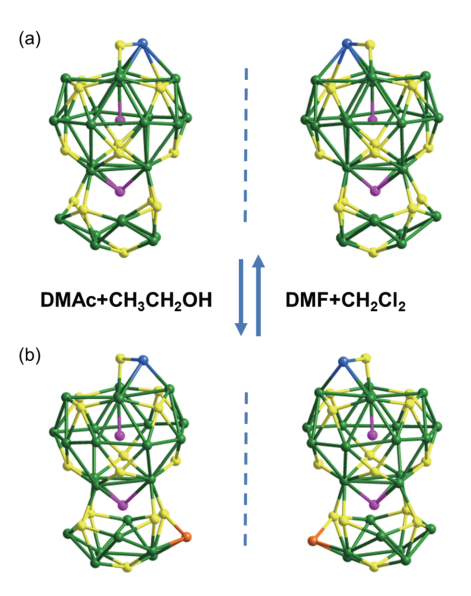


**Figure 3** Two enantiomers of the cluster of  $Ag_{25}$  (a) and  $Ag_{26}$  (b). The surface ligands were omitted for clarity (color online).

mixed solvent DMAc and  $CH_3CH_2OH$  to dissolve  $Ag_{25}$ . The resultant solution changed its colour from pale-yellow to yellow, and the crystals of  $Ag_{26}$  could be readily obtained by the diffusion method. The above experiments illustrate that the reversible transformation from  $Ag_{25}$  to  $Ag_{26}$  can be realized by the simple solvent stimuli method. Interestingly, the solvent-driven conversion process from  $Ag_{25}$  to  $Ag_{26}$  simultaneously accompanies the change in the colour of the solution, which provides a straightforward way to observe the transformation process.

The above solvent-driven reversible structure transformation between  $Ag_{25}$  and  $Ag_{26}$  can be further confirmed by the PXRD measurements. As presented in Figure S8, the observed PXRD patterns of as-synthesized  $Ag_{25}$  and  $Ag_{26}$  can be consistent with their simulated patterns. After introducing DMAc and  $CH_3CH_2OH$ , the crystal  $Ag_{25}$  got recrystallized to form a new crystal, whose PXRD patterns can well match the simulated ones of  $Ag_{26}$ . Similarly, the PXRD patterns of the crystals obtained from recrystallization of the solution  $Ag_{26}$  dissolved in mixed solvents DMF and  $CH_2Cl_2$  is consistent with the simulated ones of  $Ag_{25}$ . The above PXRD results further verified that  $Ag_{25}$  and  $Ag_{26}$  can be transformed into each other.

To investigate the details of the intermediate cluster structures in the transformation process, the positive ESI-MS was employed to study the fragments of clusters  $Ag_{25}$  and  $Ag_{26}$  in related mixed solvents. As shown in Figures S9 and S10, the solution of either  $Ag_{25}$  or  $Ag_{26}$  did not display the signal of each own molecular ions. However, they showed three same small cationic fragment peaks  $[Ag_2(Tab)-(PhCOO)]^+$  (m/z=503.9035),  $[Ag_4Cl(PhCOO)]^{2+}$  (m/z=57.4438) and  $[Ag_3(Tab)-Cl(PhCOO)]^+$  (m/z=647.7725). In addition, both clusters had their own characteristic solvent-

coordinated small cationic fragment peaks: [Ag<sub>2</sub>(Tab)<sub>2</sub>Cl- $(DMF)_2^{\dagger}$  (m/z=731.8361) and  $[Ag(Tab)_4(DMF)_2]^{\dagger}$  (m/z=731.8361)922.8483) for  $\mathbf{Ag_{25}}$ , and  $[\mathrm{Ag}(\mathrm{Tab})_3(\mathrm{DMAc})]^+$ (m/z=694.9164), and  $[Ag_2(Tab)_3(PhCOO)(DMAc)]^{\dagger}$ (m/z=924.8517) for Ag<sub>26</sub>. The disintegration of both clusters during the ESI-MS experiments implied that they were inherently dissociable in solution, which can be attributed to some weak Ag-Ag and Ag-S interactions in these Tabprotected silver nanoclusters. These results suggest that the above reversible transformation between  $Ag_{25}$  and  $Ag_{26}$  is a rare dissociation-reconstruction process involving a number of small cationic fragments, which was driven by the solvent stimuli.

The preliminary third-order non-linear optical (NLO) properties of both clusters  $\mathbf{Ag_{25}}$  in DMF and  $\mathbf{Ag_{26}}$  in DMAc were investigated by using the nanosecond Z-scan technology [13]. The Z-scan experiment was carried out with a 532 nm nanosecond laser source (Supporting Information online). The experimental curves showed typical reverse saturable absorption characteristics with a deep valley at zero point, while no obvious NLO refraction signal can be observed during the experiment (Figure 4, and Figures S13–S15). The hyperpolarizability  $\gamma$  of  $\mathbf{Ag_{25}}$  and  $\mathbf{Ag_{26}}$  could be calculated to be  $2.8 \times 10^{-30}$  and  $4.5 \times 10^{-30}$  esu, respectively. Such similar  $\gamma$  values are tentatively proposed originating from similar fragment admixtures under the experimental conditions, which may resemble those identified in abovementioned ESI-MS conditions.

In summary, we adopted Tab as the protected ligand to synthesize two chiral silver clusters,  $\mathbf{Ag_{25}}$  and  $\mathbf{Ag_{26}}$ , which have similar  $\mathbf{Ag}$ -S skeleton with different  $\mathbf{Ag}$  atom numbers. Remarkably,  $\mathbf{Ag_{25}}$  and  $\mathbf{Ag_{26}}$  clusters can be transformed into each other under the driving of solvents. By the means of PXRD and ESI-MS measurements, we can conclude that the reversible transformation of  $\mathbf{Ag_{25}}$  and  $\mathbf{Ag_{26}}$  structures was

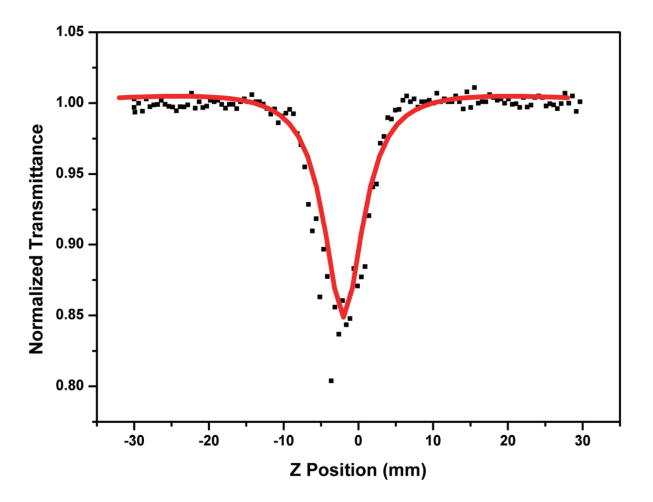


**Figure 4** View Z-scan data for  $Ag_{25}$  in DMF at 532 nm which displayed a reversed absorption. The block dots are experimental data and the red curve theoretical fit (color online).

realized through coordination solvent molecular exchange and nuclear fragmentation and rearrangement under the induction of solvent. To our knowledge, this is the first time to achieve the reversible structural transformation between two silver nanoclusters accompanying the changes in the number of silver atoms in the core structure. This work not only realizes the reversible transformation between two similar Ag clusters, but also provides a new route to synthesize new Ag clusters from the reported cluster structures.

Acknowledgements This work was supported by the National Natural Science Foundation of China (21871196, 21773163, 21531006), the State Key Laboratory of Organometallic Chemistry of Shanghai Institute of Organic Chemistry (KF2021005), Collaborative Innovation Center of Suzhou Nano Science and Technology, the Priority Academic Program Development of Jiangsu Higher Education Institutions, and the Project of Scientific and Technologic Infrastructure of Suzhou (SZS201905).

Conflict of interest The authors declare no conflict of interest.

**Supporting information** The supporting information is available online at <a href="http://chem.scichina.com">http://chem.scichina.com</a> and <a href="http://link.springer.com/journal/11426">http://chem.scichina.com</a> and <a href="http://chem.scichina.com">http://chem.scichina.com</a> and <a href="http://chem.scichina.com">http://chem.scichina.com</a>

- (a) Jin R, Zeng C, Zhou M, Chen Y. Chem Rev, 2016, 116: 10346–10413; (b) Fuhr O, Dehnen S, Fenske D. Chem Soc Rev, 2013, 42: 1871–1906; (c) Lyu D, Li J, Wang X, Guo W, Wang E. Anal Chem, 2019, 91: 2050–2057; (d) Tao Y, Li M, Ren J, Qu X. Chem Soc Rev, 2015, 44: 8636–8663; (e) Corrigan JF, Fuhr O, Fenske D. Adv Mater, 2009, 21: 1867–1871; (f) Han S, Zhang Z, Li S, Qi L, Xu G. Sci China Chem, 2016, 59: 794–801
- 2 (a) Xie YP, Jin JL, Duan GX, Lu X, Mak TCW. Coord Chem Rev, 2017, 331: 54–72; (b) Li XY, Su HF, Yu K, Tan YZ, Wang XP, Zhao YQ, Sun D, Zheng LS. Nanoscale, 2015, 7: 8284–8288; (c) Wang QM, Lin YM, Liu KG. Acc Chem Res, 2015, 48: 1570–1579; (d) Li S, Du XS, Li B, Wang JY, Li GP, Gao GG, Zang SQ. J Am Chem Soc, 2018, 140: 594–597; (e) Yang H, Yan J, Wang Y, Su H, Gell L, Zhao X, Xu C, Teo BK, Häkkinen H, Zheng N. J Am Chem Soc, 2017, 139: 31–34
- 3 (a) Zhang SS, Alkan F, Su HF, Aikens CM, Tung CH, Sun D. J Am Chem Soc, 2019, 141: 4460–4467; (b) Wu T, Yin D, Hu X, Yang B, Liu H, Xie YP, Liu SX, Ma L, Gao GG. Nanoscale, 2019, 11: 16293–16298; (c) Duan GX, Han J, Yang BZ, Xie YP, Lu X. Nanoscale, 2020, 12: 1617–1622
- 4 (a) Cho S, Jeon Y, Lee S, Kim J, Kim TH. Chem Eur J, 2015, 21: 1439–1443; (b) Guan ZJ, Hu F, Li JJ, Wen ZR, Lin YM, Wang QM. J Am Chem Soc, 2020, 142: 2995–3001; (c) Kamei Y, Shichibu Y, Konishi K. Angew Chem Int Ed, 2011, 50: 7442–7445; (d) Li Y, Cheng H, Yao T, Sun Z, Yan W, Jiang Y, Xie Y, Sun Y, Huang Y, Liu S, Zhang J, Xie Y, Hu T, Yang L, Wu Z, Wei S. J Am Chem Soc, 2012, 134: 17997–18003; (e) Liu H, Song CY, Huang RW, Zhang Y, Xu H, Li MJ, Zang SQ, Gao GG. Angew Chem Int Ed, 2016, 55: 3699–3703; (f) Wang Z, Su HF, Tung CH, Sun D, Zheng LS. Nat Commun, 2018, 9: 4407; (g) Xia N, Yuan J, Liao L, Zhang W, Li J, Deng H, Yang J, Wu Z. J Am Chem Soc, 2020, 142: 12140–12145; (h) Yao Q, Fung V, Sun C, Huang S, Chen T, Jiang DE, Lee JY, Xie J. Nat Commun, 2018, 9: 1979
- (a) Jansen M. Angew Chem Int Ed, 1987, 26: 1098–1110; (b) Schmidbaur H, Schier A. Angew Chem Int Ed, 2015, 54: 746–784;
   (c) Wang ZY, Wang MQ, Li YL, Luo P, Jia TT, Huang RW, Zang SQ, Mak TCW. J Am Chem Soc, 2018, 140: 1069–1076

- 6 Kang X, Huang L, Liu W, Xiong L, Pei Y, Sun Z, Wang S, Wei S, Zhu M. Chem Sci. 2019, 10: 8685–8693
- 7 Li S, Wang ZY, Gao GG, Li B, Luo P, Kong YJ, Liu H, Zang SQ. Angew Chem Int Ed, 2018, 57: 12775–12779
- 8 Yuan SF, Guan ZJ, Liu WD, Wang QM. Nat Commun, 2019, 10: 4032
- 9 (a) Hu F, Li JJ, Guan ZJ, Yuan SF, Wang QM. Angew Chem Int Ed, 2020, 59: 5312–5315; (b) Alhilaly MJ, Bootharaju MS, Joshi CP, Besong TM, Emwas AH, Juarez-Mosqueda R, Kaappa S, Malola S, Adil K, Shkurenko A, Häkkinen H, Eddaoudi M, Bakr OM. J Am Chem Soc, 2016, 138: 14727–14732
- 10 Bao SJ, Liu CY, Zhang M, Chen XR, Yu H, Li HX, Braunstein P, Lang JP. Coord Chem Rev, 2019, 397: 28–53
- 11 (a) Chen XR, Yang L, Tan YL, Yu H, Ni CY, Niu Z, Lang JP. Chem

- Commun, 2020, 56: 3649–3652; (b) Alhilaly MJ, Huang RW, Naphade R, Alamer B, Hedhili MN, Emwas AH, Maity P, Yin J, Shkurenko A, Mohammed OF, Eddaoudi M, Bakr OM. *J Am Chem Soc*, 2019, 141: 9585–9592
- (a) Liu C, Li T, Abroshan H, Li Z, Zhang C, Kim HJ, Li G, Jin R. Nat Commun, 2018, 9: 744; (b) Sugiuchi M, Shichibu Y, Konishi K. Angew Chem Int Ed, 2018, 57: 7855–7859; (c) Tian F, Chen R. J Am Chem Soc, 2019, 141: 7107–7114; (d) Wang Z, Liu JW, Su HF, Zhao QQ, Kurmoo M, Wang XP, Tung CH, Sun D, Zheng LS. J Am Chem Soc, 2019, 141: 17884–17890; (e) Zeng C, Liu C, Chen Y, Rosi NL, Jin R. J Am Chem Soc, 2014, 136: 11922–11925
- 13 Sheik-Bahae M, Said AA, Wei TH, Hagan DJ, van Stryland EW. IEEE J Quantum Electron, 1990, 26: 760–769